Optical diagnostic and electrical analysis in dusty RF discharges containing plasmoids

J. F. Lagrange, I. Géraud-Grenier, F. Faubert, and V. Massereau-Guilbaud

Citation: Journal of Applied Physics **118**, 163302 (2015); doi: 10.1063/1.4934249
View online: http://dx.doi.org/10.1063/1.4934249
View Table of Contents: http://scitation.aip.org/content/aip/journal/jap/118/16?ver=pdfcov
Published by the AIP Publishing

Optical diagnostic and electrical analysis in dusty RF discharges containing plasmoids

J. F. Lagrange,[1] I. Géraud-Grenier,[1] F. Faubert,[2] and V. Massereau-Guilbaud[1,a)]
[1]*GREMI, Groupe de Recherche sur l'Energétique des Milieux Ionisés, UMR 7344 CNRS/Université d'Orléans, Site de l'IUT de Bourges, 63 avenue de Lattre de Tassigny, 18020 Bourges Cedex, France*
[2]*IUT de Bourges, Département Mesures Physiques, 63 avenue de Lattre de Tassigny, 18020 Bourges Cedex, France*

(Received 24 April 2015; accepted 9 October 2015; published online 27 October 2015)

The presence of hydrogenated carbon nitride a-CN_x:H particles confined in an argon dusty discharge induces the appearance of instabilities. Those instabilities, also called plasmoids, are luminous regions which move through the plasma and rotate around the biased electrode circumference. Electrical characteristics of the plasma have been used to evidence the presence of dust particles and to demonstrate that plasmoid appearance is triggered by particles. The light emitted by the plasma is analysed by optical emission spectroscopy. This paper presents the spatial distribution of excited species, such as CN, Ar I… between electrodes both inside plasmoids and in the surrounding dusty plasma. Obtained results allow to get information for the electron energy distribution function. Moreover, the interplay between plasmoid behaviour and particle presence in the plasma is shown. © *2015 AIP Publishing LLC*. [http://dx.doi.org/10.1063/1.4934249]

I. INTRODUCTION

The presence of dust particles in plasmas is a relatively well-known phenomenon. Dusty plasmas are widely studied in order to understand particle generation, their growth, and their behaviour within the plasma bulk. The appearance of particles is very often due to the decomposition of reactive gases as, for example, silane, methane, or acetylene in plasma enhanced chemical vapor deposition (PECVD) devices.[1–4] In contact with the plasma, particles become negatively charged and stay confined in the plasma. Their presence strongly modifies the electrical and chemical properties of the discharge.[3] The electrical equilibrium of the plasma is disturbed, leading to the appearance of unstable phenomena.[5–7] Other kinds of instabilities have already been observed in dusty plasmas, such as in CF_4,[8] krypton,[5] argon discharges,[9,10] and in microgravity systems.[11–13] In this work, observed instabilities called plasmoids are likely a volume of more intense glow than its surrounding dusty plasma and they rotate along the biased electrode circumference. When the number density of grown dust particles is sufficient or particles are large enough within dusty plasma to change plasma parameters, dusty-free regions characterised by a slightly enhanced luminosity appear.[14–16] The electron trapping by particles generates an electron depleted dusty region. A dust-free and luminous region usually called void[10] or plasmoid[17] appears near the electron depleted dusty region. Due to the effect of surrounding particles, instabilities show different appearances and behaviours, such as great void mode[7] or heartbeat instabilities.[18–21]

This study presents a new experimental scenario to highlight plasmoid presence in argon dusty plasma. Experiments are carried out in low pressure radio frequency (13.56 MHz) capacitively coupled discharges at room temperature. A first discharge is obtained in a gas mixture containing 30% CH_4 and 70% N_2. Hydrogenated carbon nitride a-CN_x:H particles and coating are generated. At the end of the CH_4-N_2 discharge, the reactor is kept closed and pumped again. Then, a second experiment is carried out in argon gas. In particular experimental conditions, particles and plasmoids appear. The visual plasma observation is a way to determine conditions of instability existence. Particle presence within the discharge is put in evidence using electrical plasma parameter modifications, such as the DC self bias voltage and Laser Light Scattering (LLS). Analyse of the light emitted by the plasma is performed by Optical Emission Spectroscopy (OES). The vertical repartition of the excited species in the inter-electrode space is recorded in a same experiment both inside plasmoids and in the surrounding dusty plasma. This paper deals with the comparison between the emission line distributions of excited species in the inter-electrode space inside plasmoids and outside plasmoids, i.e., in the dust regions. Obtained results also allow to get information about the Electron Energy Distribution Function (EEDF) inside plasmoids and in the surrounding dusty plasma. Moreover, the plasmoid behaviour, their interaction with dust clouds, and their influence on the DC self bias voltage are shown. Results are discussed in the last part.

II. EXPERIMENTAL SETUP AND PROTOCOL

The experimental setup has been described in previous papers.[22,23] A radio frequency (13.56 MHz) capacitively coupled discharge is ignited between two parallel plane electrodes in a stainless steel reactor. The upper electrode (13.5 cm in diameter) is polarised and the lower electrode (20 cm in diameter) is grounded as well as the reactor wall. The distance between electrodes is about 2.5 cm. Gases are injected perpendicularly to the vertical axis of the reactor

a)Author to whom correspondence should be addressed. Electronic mail: Veronique.massereau@univ-orleans.fr

near the electrodes. Viewports in the chamber sidewall allow discharge observations and discharge measurements. The 13.56 MHz radio frequency generator (Huttinger, PFG 300) is capacitively coupled to the top electrode through a matching network (Huttinger, PFM 1500A). As surface areas of the biased electrode and the grounded one are asymmetric, a negative DC self-bias voltage (V_{DC}) appears between the electrodes. Its temporal evolution is recorded with an oscilloscope (Tektronix DPO5034). A vertically expanded laser beam (Ar^+ laser, $\lambda = 514.5$ nm) is directed through the reactor parallel to the electrodes. The LLS is used in order to observe the particle presence and behaviour within the plasma bulk. With this laser wavelength, only particles with a diameter greater than 50 nm can be observed. The scattering light coming from particles is recorded with a camera (Sony, DSC-HX50), perpendicularly to the laser beam.

The different excited species within the plasma bulk are detected by optical emission spectroscopy. Plasma emission spectra in the wavelength range from 300 to 850 nm are recorded through a viewport using a bundle of 30 optical fibers, lenses, and a spectrometer coupled with a charge coupled device camera Princeton Instruments. Each optical fiber is 400 nm in diameter. The lenses are used to focus plasma light on the fibers. With this spectroscopic setup and its magnification, a plasma slice of 1.2 mm of width and 2.5 cm of height (inter-electrode space) is analysed. Thus, temporal line intensities are simultaneously measured in the inter-electrode space. In order to have a chance to acquire light from plasmoids or from the surrounding dusty plasma, exposure time is set to 50 ms, and the instability speed is the lowest possible.

In order to obtain instabilities in argon discharge, a particular protocol has been established:

(1) The electrodes and the reactor walls are cleaned with ethanol and sand paper.
(2) The reactor is pumped until reaching a residual pressure lower than 10^{-3} Pa.
(3) The cleaned reactor is filled with a working gas mixture containing 30% CH_4 and 70% N_2 with a constant total gas flow rate of 5.6 sccm. The pressure for particle production is 120 Pa. The RF power is set at 80 W and the experiment time is 25 min. During this first experiment, hydrogenated carbon nitride particles are generated inside the chamber and a coating grows on the biased electrode. In this third step, we obtain a "polluted chamber."
(4) At the end of the CH_4-N_2 discharge, the reactor is kept closed. The vacuum chamber is again pumped to a residual pressure lower than 10^{-3} Pa.
(5) The second experiment is carried out in argon gas. The chamber is filled with an argon pressure ranging from 50 to 60 Pa with a constant total gas flow rate of 5.6 sccm. The experiment is now done with an RF power of 40 W. We can notice that pressure and power are different in an argon discharge from those in a CH_4-N_2 discharge. Firstly, the working pressure has been chosen for plasmoid appearance, and then the power has been adjusted in order to have a DC self-bias voltage in the same range values both in CH_4-N_2 and in argon discharges.

III. NEW STUDY OF DUST AND PLASMOIS IN ARGON DISCHARGE

According to the experimental protocol, a first discharge is realised in CH_4-N_2 gas mixture. In such gas mixtures, particle generation and coating growth on the biased electrode have been investigated in detail in previous studies.[23–25] Particle and coating growth come from the dissociation of methane and nitrogen during the discharge, leading to the formation of CH_x and CN radicals. Radicals are the main material source for particle formation and coating growth on the biased electrode. Chatei *et al.*[26] have shown, under similar experimental conditions, that CH radicals come from the plasma bulk. Atomic hydrogen can also come from the ejection of adsorbed hydrogen atoms as a result of ion–surface collisions.[27] The physical and/or chemical sputtering[28,29] of coating and particles by N_2^+ ions leads to a release of volatile compounds, such as CN and C_2N_2 radicals.

In low pressure plasmas, particles become negatively charged resulting from the balance between electron flux and ion flux hitting particles.[30] Due to this negative charge and under different force actions,[31] i.e., gravity, thermophoresis, electrostatic, electric, and ion drag forces, particles remain confined in the plasma and levitate into two well-defined dust clouds near the sheath boundaries. The particle dust clouds are parallel to the electrodes, their form follows the electrical field lines.

As can be seen in Figure 1(a), particles firstly appear near the biased electrode and are trapped in a dust cloud at the RF sheath boundary. When they reach a critical size, the gravity and the thermophoresis forces increase, leading to the particle fall throughout the plasma bulk. Then, particles levitate above the grounded electrode (Fig. 1(b)).

Particles created in CH_4-N_2 gas mixture are collected at the end of some experiments to observe them using Scanning Electron Microscopy (SEM). As can be seen in Figure 2(a), particles have a spherical shape (up to 2 μm in size) and a rough surface often called a cauliflower shape.

Simultaneously with the particle generation, a coating grows on the biased electrode surface. The coating is not very adhesive. Thus, some fragments can fall during the experiment and can also levitate at the sheath boundaries.

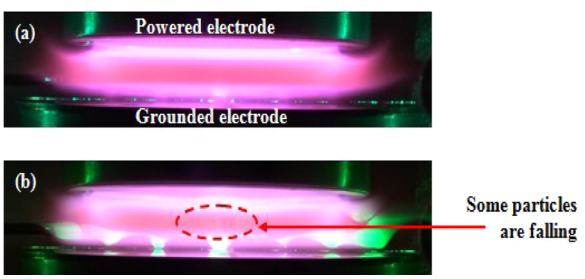

FIG. 1. Pictures of discharges in CH_4-N_2 gas mixture. (a) Particles, in green, are growing below the biased electrode. (b) Particles in green are still growing below the biased electrode, some particles fall and other ones levitate above the grounded electrode.

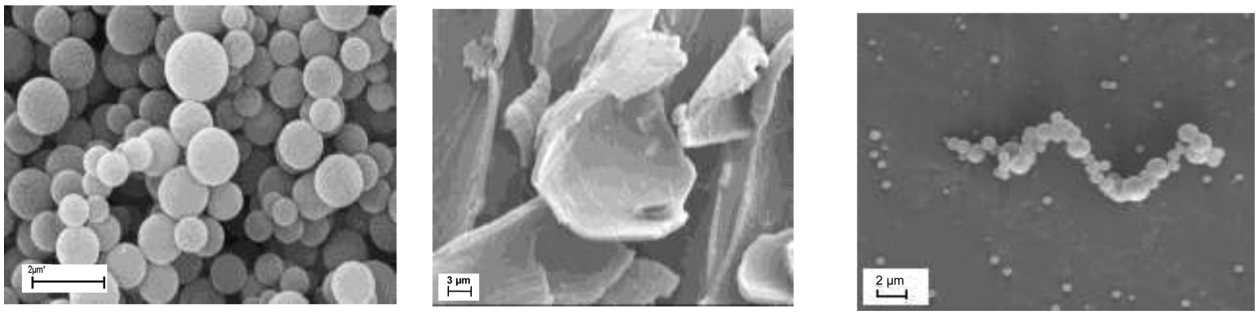

FIG. 2. (a) SEM picture of particles produced in CH_4-N_2 gas mixture, (b) SEM picture of coating fragments, and (c) SEM picture of particles produced in argon gas.

Fragments have a specific brown colour and a SEM picture (Fig. 2(b)) shows that they have a dimension up to one hundred micron long.

After the production of particles and coating in CH_4-N_2 gas mixture, another discharge in pure argon is carried out (5th step of the experimental protocol). In this second experiment, some particles appear within the discharge. The particle cloud that appears in argon plasma comes from the setting in motion of particles previously formed in CH_4-N_2 plasma and from the sputtering of the coating on the biased electrode. A SEM picture of particles obtained is presented in Figure 2(c). Particles present a similar shape than particles obtained in CH_4-N_2 gas mixture. As less particles are produced, we collect less particles as shown in Figure 2(c). CN and CH radicals come from the sputtering by positive argon ions of the coating of the biased electrode and of the particles. The CH and CN radicals can be adsorbed by particles already present in the plasma bulk, leading to their growth in argon discharge. Moreover, these radicals can induce a new particle generation in argon discharge. For example, molecular precursors are released in neutral gas (Ar, He) discharges, where a polymer (usually melamine formaldehyde)[12,32–34] or graphite[35,36] is sputtered.

After a moment, depending on the experimental conditions, plasmoids appear within the plasma. For example, for an RF power of 40 W and a pressure of 60 Pa, plasmoid appearance occurs a few minutes after the plasma is on. Under other experimental conditions, this time can be less than 1 min. As can be seen in Figure 3(a), plasmoids are characterised by a slightly enhanced luminosity, and look like "oval" bright plasma balls with an average width size of 2 cm and a length size of 2.5 cm (inter-electrode distance) (Fig. 3(a)). They move in the inter-electrode space and rotate along the biased electrode circumference in the clockwise direction. They are equidistant from each other during their rotation. We have never observed plasmoids in a totally clean vacuum chamber, i.e., without previous coatings and particles. For pressures lower than 40 Pa, no particles are detected by LLS and no plasmoids are observed (Fig. 3(c)). We have carried out several experiments in different conditions of pressure, RF powers, and vacuum chamber cleanliness. We have noticed that plasmoid behaviour becomes more and more complex with the increased number of particles. Similar observations have been reported by Mikikian *et al.*[5] We have also noticed that the number of plasmoids and their rotation velocity are increasing with increasing either power or gas flow. For example, for RF powers between 40 and 100 W, the number of plasmoids ranges from 1 to 5, and the rotation frequency ranges from 0.5 to 3 Hz. As the RF electrode is 13.5 cm in diameter, the average speed of plasmoids varies between 0.3 m/s and 1.2 m/s. These results are in agreement with the literature:[22] Experimental conditions play an important role in the number and the speed of the plasmoids. Finally, looking at Figure 3(b), we notice that plasmoids and levitating particles push away each other due to the ion drag force. Other kind of rotating instabilities has also been observed in different studies: for example, in an argon-helium discharge containing acetylene at the beginning of the experiment[7,17] or in an argon RF plasma where graphite targets are sputtered.[10]

Voids and plasmoids are more intense luminous regions in dusty plasma. Usually, in dusty plasmas, the void appearance occurs in the plasma centre and only one void is observed.[7,11,20,21,37] The high gradient in electron number density between a void and surrounding dusty plasma induces the appearance of an electric field causing the electron transport inward void and the positive ions transport in dust clouds. Voids are formed when the outward ion drag force on the dust particles driven by an ambipolar ion flux becomes larger than the inward electrostatic force due to the negative particle charge.[10,38,39] The ion drag force pushes

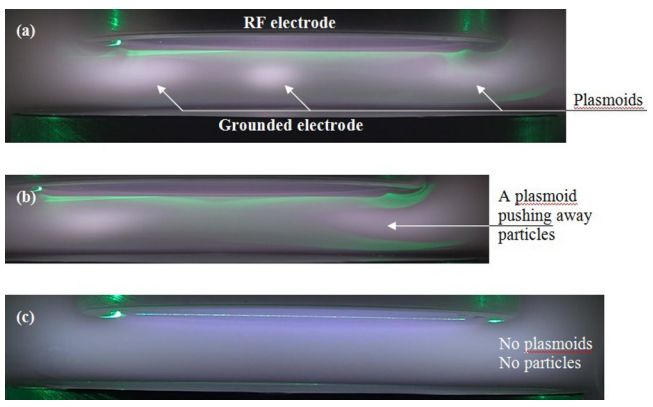

FIG. 3. (a) Three plasmoids in a dusty argon discharge; particles in green. (b) A plasmoid enters the particle slice. (c) No particles and no plasmoids are visible.

particles outside void. Many theoretical studies correlated with experimental results have been carried out to understand the void formation[40,41] and the void collapse.[42,43] Moreover, when a void rotates around the vertical axis of the discharge, it is just off-centered and a part of the void remains in the plasma centre. Plasmoids are also dust free region but not necessary linked to the centre of the discharge. Plasmoids rotate in the discharge. One or more plasmoids can be present in the discharge. In our case, there are no luminous plasma balls in the plasma centre: the luminous plasma ball that we see in the middle of Figure 3(a) is located in the background at the periphery of the biased electrode. No particles are detected inside our luminous plasma balls by LLS. Nevertheless, as LLS is done using a wavelength of 514.5 nm, only particles with a diameter over 50 nm can be highlighted. Moreover, we observe several luminous plasma balls that are not formed from the plasma centre. Our instabilities show typical characteristics of plasmoids surrounding by dusty plasma.

To try to explain the plasmoid rotation, we have done different experiments by changing the direction of the gas injection between electrodes: The injection of gas is performed either along the vertical axis of the reactor or either perpendicular to this axis. No changes have been observed for the rotation of the plasmoids and they always rotate in the same direction. Schulze *et al.*[37] have studied the rotation of a void in an argon/neon/acetylene dusty discharge. They have shown that a weak magnetic field is required to generate the rotation of the void. Without magnetic field, the void is located at the reactor centre. When a weak magnetic field is applied, the tangential component of the ion drag force is exhibited: The particles located around the void rotate inducing the void rotation. In our experimental setup, the only magnetic field that exists comes from the cold cathode gauge used to control the pressure before experiments. If we make a parallel with Schulze *et al.*,[37] the plasmoid rotation could be explained by the existence of this weak magnetic field. Further analyses are still in progress.

IV. DC SELF BIAS VOLTAGE

In low pressure dusty plasmas, electron trapping by particles leads to time variations of electrical parameters, such as the DC self bias voltage. In previous studies,[3,22,23] time variations of the DC self bias voltage (V_{DC}) have been linked to particle presence and behaviour below the biased electrode. Modifications of the DC self bias voltage are dependent on the electron number trapped by particles. The trapped electron number depends on particle size and on particle number density. Time evolutions of the DC self bias voltage are recorded according to the different steps of the experimental protocol: Firstly, in a CH_4-N_2 discharge during the particle production, and secondly, in an argon discharge. Figure 4 shows time evolutions of the DC self bias voltage: (a) in CH_4-N_2 discharge, (b) in an argon discharge containing plasmoids, (c) in an argon discharge without plasmoid.

In the 30% CH_4 −70% N_2 gas mixture, time variations of the V_{DC} have already been correlated with a multi-generation of particles in a previous study.[23] As can be seen in Figure 4(a), V_{DC} increases from −100 V to −85 V during the first 80 s of the experiment. The V_{DC} enhancement corresponds to a first particle generation. Then, V_{DC} decreases when particles go downward (decrease in about 20 V), i.e., the dust cloud below the biased electrode empties. These phenomena occur a second time between 200 and 300 s and correspond to a second particle generation. Finally, for times over 500 s, no more particles are generated.

According to the experimental protocol, the fifth step is now realised: A discharge in argon gas is supplied in a reactor polluted by the particles and the coating on the biased electrode. Time evolution of the DC self-bias voltage (Fig. 4(b)) shows that V_{DC} begins to increase about 20 s after

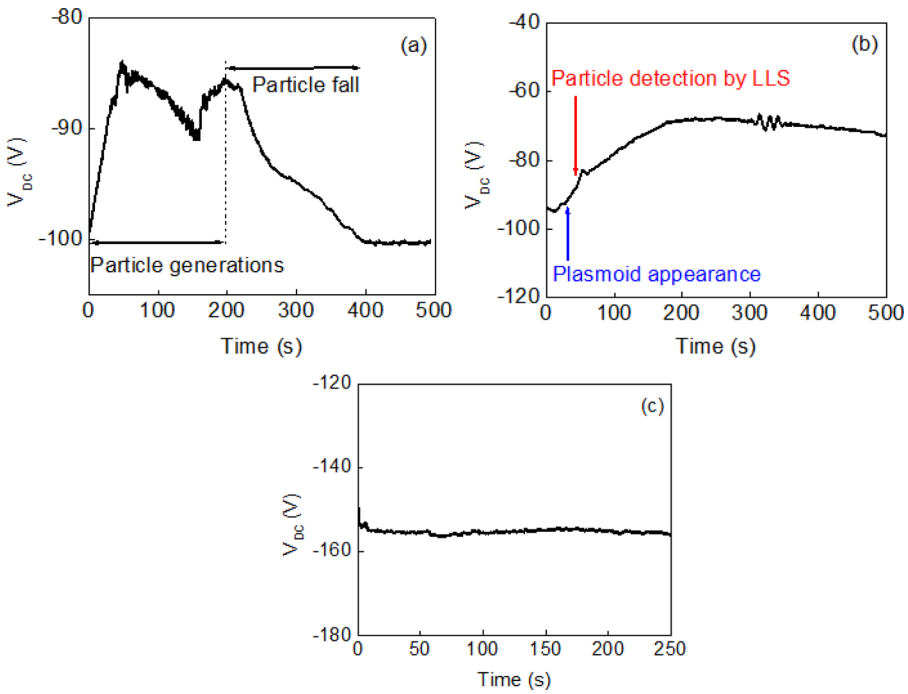

FIG. 4. Time evolution of the DC self-bias voltage in (a) CH_4-N_2 discharge ($P_{CH4\text{-}N2} = 120$ Pa; $P_{RF} = 80$ W), (b) dusty argon discharge ($P_{Ar} = 50$ Pa; $P_{RF} = 40$ W), and (c) dusty-free argon discharge ($P_{Ar} = 35$ Pa; $P_{RF} = 40$ W).

TABLE I. Spectroscopic characteristics of the observed lines for atomic species.

	Wavelength (nm)	Level configurations	Excitation energy (eV)
Ar I	801.47	3s23p5(2P°3/2)4p → 3s23p5(2P°3/2)4s	13.09
Ar II	427.75	3s23p4(1D)4p → 3s23p4(1D)4s	21.3
H (alpha)	656.28	…	12.1

the power is on. Then, V_{DC} increases from −94 V to about −68 V until 200 s. For time over 200 s, low variations of the V_{DC} are observed. In Figure 4(b), the time corresponding to the plasmoid appearance is indicated: Plasmoids appear in the discharge after the beginning of the V_{DC} increase. Moreover, we have also reported in Figure 4(b) the time corresponding to the beginning of particle detection by laser light scattering below the biased electrode. The particle detection by LLS occurs after the appearance of plasmoids.

As can be seen in Sec. III, plasmoids and particles do not appear in a "polluted reactor" for an RF power of 40 W and a pressure lower than 40 Pa. As it is shown in Figure 4(c), when no particles are visible and when no plasmoid appears, the V_{DC} time evolution stays almost constant during the discharge.

V. OPTICAL EMISSION SPECTROSCOPY

Optical emission spectroscopy measurements are made between the electrodes, in order to get the emission line distribution of excited species within the inter-electrode space. Spectra are recorded for each wavelength during a same experiment with a number of 100 frames. The optical detection system is calibrated by a tungsten lamp to determine intensity correction factors. The spectroscopic characteristics of the different emission lines observed in the 300–850 nm spectral range are shown in Table I for atomic species and in Table II for molecular species. In an argon discharge, as plasmoids rotate within the discharge along the biased electrode circumference, it is not possible to choose the moment when a plasmoid is present or not in front of the viewport for measurements. Nevertheless, it is possible to record spectra inside a plasmoid or outside a plasmoid during a same experiment because

– OES measurements have been done with two plasmoids in the reactor;
– Series of 100 frames are recorded with a repetition rate of 3 Hz, whereas the maximum of the rotation frequency of plasmoids is about 0.8 Hz;

TABLE II. Spectroscopic characteristics of the observed lines for molecular species.

	Head band wavelength (nm)	Level configurations	Band (v′, v″)	Excitation energy (eV)
N_2	337.1	$C\ ^3\Pi_u \rightarrow C\ ^3\Pi_u$	(0, 0)	11.1
N_2^+	391.44	$B\ ^2\Sigma^+_u \rightarrow X\ ^2\Sigma^+_g$	(0, 0)	18.7
CH	431.42	$A\ ^2\Delta \rightarrow X\ ^2\Pi$	(0, 0)	2.9
CN	387.14	$B\ ^2\Sigma \rightarrow X\ ^2\Sigma$	(0, 0)	3.3

– Each plasmoid is 2 cm in width, whereas the circumference of the biased electrode is 42 cm (13.5 cm in diameter);
– The time resolution is 50 ms and the width slice of the analysed plasma is 1.2 mm.

The emitted light is much more important inside plasmoids than in the surrounding plasma. All spectra are studied and selected as a function of their emitted light. Thus, we obtain spectra corresponding to the spectroscopic analysis inside a plasmoid or outside a plasmoid in a dusty argon discharge.

Spatial distributions of emission lines between electrodes are shown in a CH_4-N_2 discharge (Fig. 5) and in an argon discharge containing particles and coating (Fig. 6). The species detected by optical emission spectroscopy are

– H_{alpha}, N_2, N_2^+, CH, and CN in a CH_4-N_2 discharge.
– Ar I, Ar II, H_{alpha}, CH, and CN in an argon dusty discharge.

During the particle production process in CH_4-N_2 gas mixture, the emission spatial profile exhibits two distinct emission peaks between electrodes (Fig. 5), near sheath boundaries. The maximum of the more intensive peak is about 7.5 mm from the biased electrode, whereas the maximum of the less intensive peak is about 4.5 mm from the grounded electrode. The line intensity of excited CH radical is too weak to be visible in the background noise. We have shown in a previous paper[25] that CH emission line intensity is negligible during experiments in nitrogen-rich plasmas. Methane proportion in the gas mixture is low, CH radicals and their precursors are consumed by particles and coating growth. A similar result has been obtained by Wang *et al.*[44]

In argon dusty discharges, the spatial distributions of the emission lines of Ar I, Ar II, H_{alpha}, CH, and CN species are different from those obtained in CH_4-N_2 discharges. CH and CN radicals are of interest because they take part in the formation of coatings and particles. However, as in CH_4-N_2 discharge, CH lines have a weak intensity and are almost completely obscured by a significant background noise. Only Ar I, Ar II, H_{alpha}, and CN emission line evolutions are reported in Figure 6. The line intensities of excited species are higher inside plasmoids than in the surrounding dusty plasma: for example, a multiplicative factor of 8.5 for CN and H_{alpha} lines and a multiplicative factor of 3 for Ar I. Moreover, the spatial distributions of lines inside and outside plasmoids are different:

– Outside plasmoids:
  Atomic lines of Ar I and Ar II species in argon discharge reach a maximum value near the biased electrode, i.e., about 7–8 mm. Head line distribution of H_{alpha} and CN

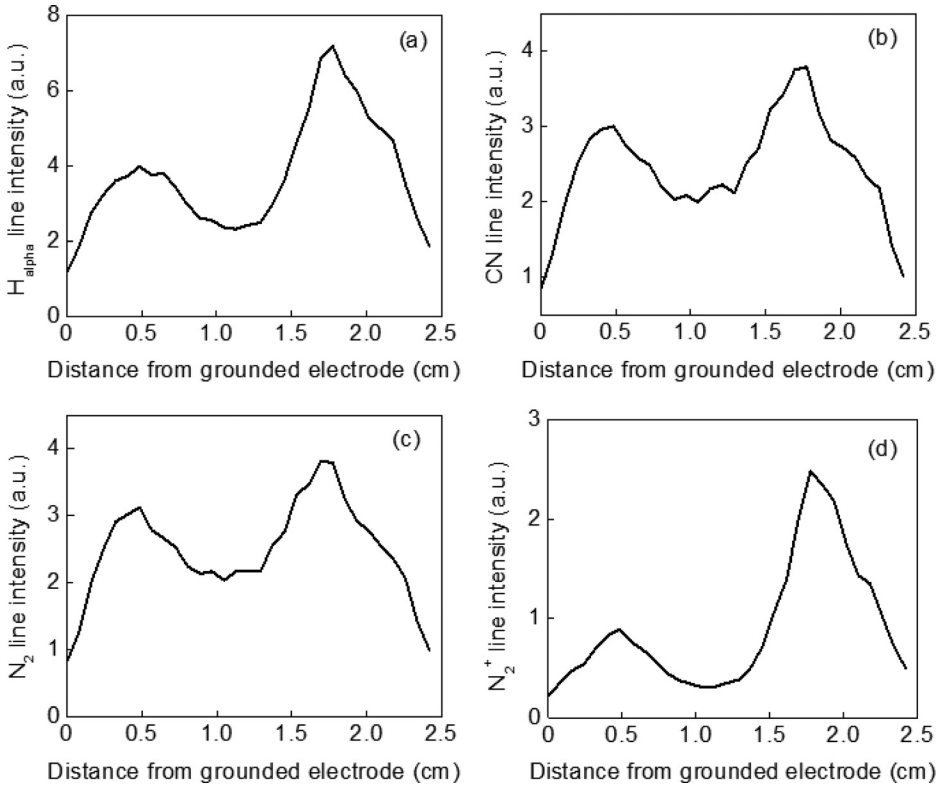

FIG. 5. Vertical line intensity repartition between electrodes spaced apart by 2.5 cm in CH_4-N_2 gas mixture (30% CH_4 −70% N_2) for (a) H_{alpha} (656.2 nm), (b) CN (387.1 nm), (c) N_2 (337.1 nm), and (d) N_2^+ (391.4 nm).

species reaches its maximum value near the middle of the inter-electrode space about 13 mm from the biased electrode.

– Inside plasmoids:
Ar I, H_{alpha}, and CN species are mostly excited in the middle of the inter-electrode space, which corresponds to the middle of plasmoids. Ar II lines show the same distribution inside or outside plasmoids and reach a maximum value about 6 mm from the biased electrode.

VI. DISCUSSION

In dusty argon discharge, for pressures lower than 40 Pa, no particles with a diameter greater than 50 nm are detected

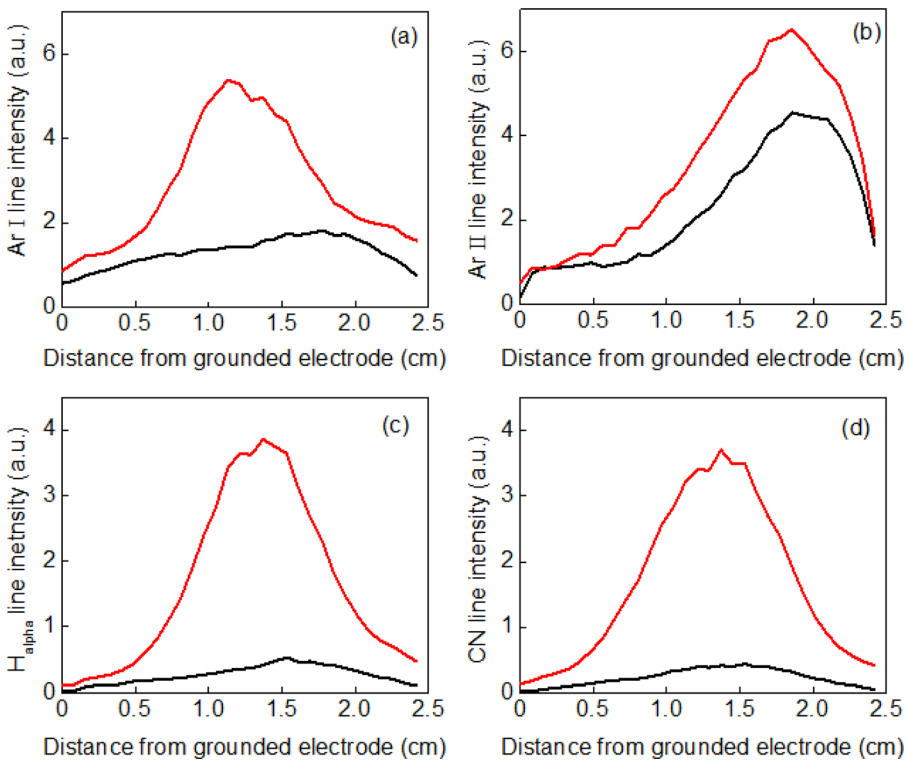

FIG. 6. Vertical line intensity repartition between electrodes spaced apart by 2.5 cm inside instabilities (red curve) and outside plasmoids (dark curve) in a same dusty argon discharge for (a) Ar I (801.47 nm), (b) Ar II (427.7 nm), (c) H_{alpha} (656.2 nm), and (d) CN (387.1 nm).

by laser light scattering and no plasmoids are visible within the plasmas bulk (Fig. 3(c)). In the same time, DC self bias voltage remains constant (Fig. 4(c)) meaning that no particles are present in the argon discharge.

In dusty argon discharge, for pressures over 40 Pa, the following chronology has been observed for different experimental conditions of pressure and RF power (Fig. 4(b)):

– the V_{DC} enhancement at the beginning of the experiment (time ≈ 10 s) reveals the particle presence in a dusty argon discharge;
– at time ≈ 30 s, plasmoids appear;
– at time ≈ 40 s, particles with diameter over 50 nm are detected by LLS.

As plasmoids appear before the particle detection by LLS, we can conclude that the plasmoid appearance is triggered by particles less than 50 nm in size. Some studies have shown a correlation between particle size and plasmoids.[7,15] Moreover, particle and plasmoid appearance depend on the experimental conditions so on the number and the energy of the argon ions. If ions are not able to generate particles, plasmoids can not appear. Further experiments will be carried to study this point.

In this study, OES is used to highlight the vertical distributions of excited species in plasmoids and in the surrounding dusty plasma. OES measurements have been carried out both in a CH_4-N_2 discharge and in a dusty argon discharge containing plasmoids (3rd and 5th step in the experimental protocol). In a CH_4-N_2 discharge, detected excited species are N_2 and N_2^+, CN, CH, and H_{alpha}. In a dusty argon plasma containing plasmoids, excited species detected are CH, CN, H_{alpha}, Ar I, and Ar II.

The spatial profile of line intensities in CH_4-N_2 discharge (Fig. 5) exhibits two pronounced maxima located near the electrodes. In the same place, particles levitate in dust clouds. The intensity difference results from the dissymmetry of the discharge due to the uneven effective electrode areas (the grounded electrode is larger than the biased one). Similar inter-electrode repartition has been observed by Tachibana *et al.*[45] for a pressure of 65 Pa: the emission spatial profiles reflect the evolution of the electron population near sheaths. If we look now at a dusty argon discharge, particles fill the plasma bulk. The spatial profile of the line intensity inside instabilities or outside instabilities presents a single maximum. According to Perrin *et al.*,[46] the spatially resolved optical emission shows the characteristic transition from collisional "wave-riding" on the sheath boundaries to "Joule heating" in the plasma bulk.

Recorded line intensities of CN, H_{alpha}, Ar I, and Ar II excited species are higher in plasmoids than in the surrounding dusty plasma (Fig. 6). Theoretical studies[43,47] show that the plasma density is more important inside a void than in the electron depleted dust region. In the electron depleted dust region, a larger electric field is required to generate the RF current to sustain the discharge: electrons are heated in dust region. Thus, the energy flux is transported by the inward pointing electrical field from the dust region to the void centre and is lost in void, causing ionisation and excitation. Thus, luminosity is more important in void than in the surrounding dusty plasma. The increase in the plasma emission inside voids has been observed in many cases[7,10,16,48] by optical emission spectroscopy. Our results are consistent with a greater electron number density in plasmoids, leading to an enhancement of the excitation and the ionisation. Excited species line intensities depend on the number of non-excited species and on their excitation energy. We recall that the sputtering of both the coating on the biased electrode and the particles releases non-excited species, such as CN, CH, and H_{alpha}. We have shown that there are no particles with diameter higher than 50 nm in our plasmoids. It is unlikely that the number of non-excited species is more important inside plasmoids than in the surrounding dusty plasma. Consequently, it is necessary to take into account the excitation energy of the non-excited species. Although OES measurements do not give the real electron energy distribution function, they allow to evidence EEDF changes inside plasmoids and in the surrounding dusty plasma. In our experiments, excitation energy of CN, H_{alpha}, Ar I (see Tables I and II) is up to 13 eV, whereas the ionisation energy for Ar II is 15.7 eV and its excitation energy is equal to 21 eV. In order to find a correlation between the electron excitation energy and the increase in the line intensity inside plasmoids, we have reported in Figure 7 the line intensity distribution in the inter-electrode space for the excited species Ar I (425.93 nm) whose electron excitation energy is 14.7 eV.

We notice that the vertical line distribution presents the same shape as Ar I (801.47 nm), CN, and H_{alpha} species. The maximum value is located in the middle of the inter-electrode space, i.e., in the middle of a plasmoid. The maximum of emission lines in the centre of a plasmoid is consistent with theoretical and experimental studies,[7,47] showing that the electron number density is higher in the centre of a void. Consequently, the maximum of ionization and excitation occurs in the centre of a void. In our case, ionization and excitation are more important in the middle of plasmoids for electrons with excitation energy less than 15 eV. The results seem to show a correlation between the increase in the line

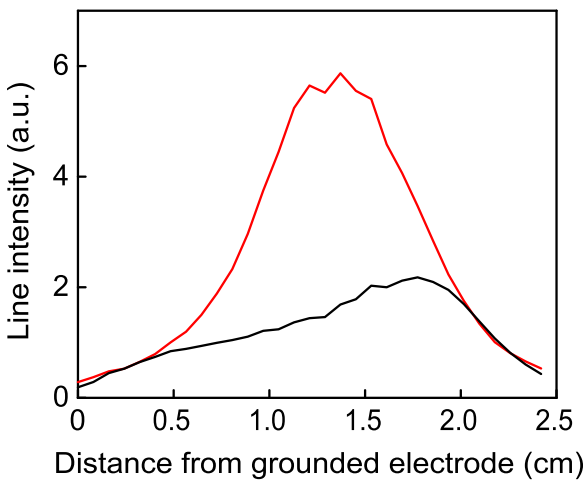

FIG. 7. Vertical line intensity repartition between electrodes spaced apart by 2.5 cm inside plasmoids (red curve) and outside plasmoids (dark curve) in the same dusty argon discharge for Ar I (425.9 nm).

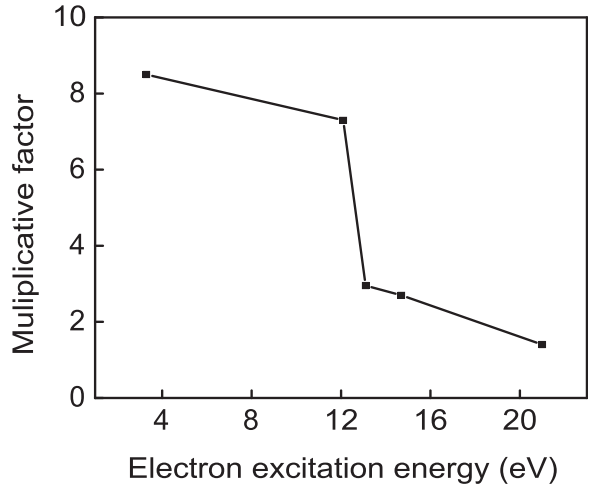

FIG. 8. Ratio between the maximum value of the line intensity inside a plasmoid and the maximum value of the line intensity in the surrounding dusty plasma as a function of the electron excitation energy.

intensities inside plasmoids and the electron excitation energy. To confirm this assumption, a multiplicative factor between the maximum value of the line intensity inside a plasmoid and the maximum value of the line intensity in the surrounding dusty plasma for each excited species is calculated. This multiplicative factor is represented for the following excited species Ar II, Ar I (801.47 nm), Ar I (425.9 nm), CN, and H_{alpha} versus their electron excitation energy in Figure 8. It is decreasing with the electron energy excitation increasing. A significant change of slope is observed around 12 eV. In plasmoids, a strong increase in the population of the excited levels, with excitation energy up to 12 eV, is clearly induced. These results show that the EEDF is significantly disturbed along the vertical axis by the plasmoid presence for electrons with energy up to 12 eV. As a consequence, the electron number density with a low energy (up to 12–15 eV) is higher in the middle of the inter-electrode space, i.e., in the middle of the plasmoids than in the surrounding dusty plasma. On the other hand, for electrons with energy greater than 15 eV, the enhancement is less important. Nevertheless, for electron excitation energy around 21 eV, the plasmoid presence does not modify the spatial line intensity repartition between the electrodes. The value of the line intensity is very weakly increased. So, the electron number density with energy higher than 15 eV is not disturbed by the plasmoid presence in the discharge.

VII. CONCLUSION

This paper describes a new scenario to generate plasmoids in dusty argon discharge with a not fully clean vacuum chamber and presents optical emission spectroscopic analyses both inside plasmoids and in the surrounding dusty region. The plasmoid presence strongly depends on the argon pressure. Up to 40 Pa, in a dust-free argon plasma, no instabilities are visible. Whereas with increasing argon pressure, above 40 Pa, they appear in the inter-electrode space and start to rotate along the biased electrode circumference. In the same time, particles are detected by LLS and the DC self bias voltage values vary during the experiment. We have shown that the plasmoid appearance is triggered by the levitated a-CN_x:H particles less than 50 nm in size.

By optical emission spectroscopy, it has been shown that in the inter-electrode space, spectral line profiles of CN, H_{alpha}, Ar I, and Ar II excited species present different shapes in dusty CH_4-N_2 plasma, and in the dusty argon plasma. In dusty CH_4-N_2 plasma, the spectral line profile presents two dominant peaks, whereas in dusty argon plasma, the spectral line profile presents only one peak. In plasmoids, the peak is localised in the middle of the inter-electrode space, i.e., in the centre of plasmoids due to enhanced ionisation and excitation.

Using all emission lines, a wide range of electron energy is sensed. In this manner, we obtain information on the electron energy distribution function. It has been established that the EEDF is modified in plasmoids for electrons whose excitation energy is up to 12 eV: a greater electron number density and a modification in the spatial distribution of the electrons in the inter-electrode space. Nevertheless, weak modifications are observed for electrons with higher energies (21 eV): The line intensities are hardly disturbed and the spatial distribution remains identical.

ACKNOWLEDGMENTS

This work has been financially supported by Agence Nationale de la Recherche, INDIGO project (ANR-11-JS09-010-01). The authors are grateful to Maxime Mikikian for all the interesting discussions about dusty plasmas and plamoids. They also thank Jean Benerdjak for his technical assistance.

[1]A. Bouchoule and L. Boufendi, Plasma Sources Sci. Technol. **2**, 204 (1993).
[2]C. Deschenaux, A. Affolter, D. Magni, C. Hollenstein, and P. Fayet, J. Phys. D: Appl. Phys. **32**, 1876 (1999).
[3]I. Géraud-Grenier, V. Massereau-Guilbaud, and A. Plain, Eur. Phys. J.: Appl. Phys. **14**, 187 (2001).
[4]V. Massereau-Guilbaud, I. Géraud-Grenier, and A. Plain, Eur. Phys. J.: Appl. Phys. **11**, 71 (2000).
[5]M. Mikikian, H. Tawidian, and T. Lecas, Phys. Rev. Lett. **109**, 245007 (2012).
[6]M. Mikikian, H. Tawidian, and T. Lecas, IEEE Trans. Plasma Sci. **42**, 2670 (2014).
[7]M. Schulze, A. V. Keudell, and P. Awakowicz, Plasma Sources Sci. Technol. **15**, 556 (2006).
[8]T. Wegner, C. Kullig, and J. Meichsner, IEEE Trans. Plasma Sci. **42**, 2572 (2014).
[9]M. Mikikian, L. Couedel, Y. Tessier, and L. Boufendi, IEEE Trans. Plasma Sci. **39**, 2748 (2011).
[10]D. Samsonov and J. Goree, Phys. Rev. E **59**, 1047 (1999).
[11]B. Buttenschon, M. Himpel, A. Melzer, D. Caliebe, and K. O. Menzel, IEEE Trans. Plasma Sci. **39**, 2754 (2011).
[12]M. Mikikian, L. Boufendi, A. Bouchoule, H. M. Thomas, G. E. Morfill, A. P. Nefedov, V. E. Fortov, and PKE-Nefedov Team, New J. Phys. **5**, 19 (2003).
[13]A. P. Nefedov, O. S. Vaulina, O. F. Petrov, V. I. Molotkov, V. M. Torchinskii, V. E. Fortov, A. V. Chernyshev, A. M. Lipaev, A. I. Ivanov, A. Y. Kaleri, Y. P. Semenov, and S. V. Zaletin, New J. Phys. **5**, 108 (2003).
[14]J. L. Dorier, C. Hollenstein, and A. A. Howling, J. Vac. Sci. Technol. A **13**, 918 (1995).
[15]J. Goree, G. Morfill, V. Tsytovich, and S. Vladimirov, Phys. Rev. E **59**, 7055 (1999).
[16]G. Praburam and J. Goree, Phys. Plasmas **3**, 1212 (1996).

[17]J. Schulze, D. Luggenholscher, and U. Czarnetzki, IEEE Trans. Plasma Sci. **36**, 1402 (2008).
[18]M. R. Akdim and W. J. Goedheer, IEEE Trans. Plasma Sci. **32**, 680 (2004).
[19]R. J. Heidemann, L. Couëdel, S. K. Zhdanov, K. R. Sütterlin, M. Schwabe, H. M. Thomas, A. V. Ivlev, T. Hagl, G. E. Morfill, V. E. Fortov, V. I. Molotkov, O. F. Petrov, A. I. Lipaev, V. Tokarev, T. Reiter, and P. Vinogradov, Phys. Plasmas **18**, 053701 (2011).
[20]M. Mikikian, L. Couëdel, M. Cavarroc, Y. Tessier, and L. Boufendi, New J. Phys. **9**, 268 (2007).
[21]M. Y. Pustylnik, A. V. Ivlev, N. Sadeghi, R. Heidemann, S. Mitic, H. M. Thomas, and G. E. Morfill, Phys. Plasmas **19**, 103701 (2012).
[22]V. Massereau-Guilbaud, J. Pereira, I. Géraud-Grenier, and A. Plain, J. Appl. Phys. **105**, 033302 (2009).
[23]J. Pereira, V. Massereau-Guilbaud, I. Géraud-Grenier, and A. Plain, J. Appl. Phys. **103**, 033301 (2008).
[24]J. Pereira, I. Géraud-Grenier, V. Massereau-Guilbaud, and A. Plain, Thin Solid Films **482**, 226 (2005).
[25]J. Pereira, V. Massereau-Guilbaud, I. Géraud-Grenier, and A. Plain, Plasma Process. Polym. **2**, 633 (2005).
[26]H. Chatei, J. Bougdira, M. Remy, and P. Alnot, Surf. Coat. Technol. **116–119**, 1233 (1999).
[27]S. B. Radovanov, K. Dzierżęga, J. R. Roberts, and J. K. Olthoff, Appl. Phys. Lett. **66**, 2637 (1995).
[28]A. A. Fridman, L. Boufendi, T. Hbid, B. V. Potapkin, and A. Bouchoule, J. Appl. Phys. **79**, 1303 (1996).
[29]T. Schwarz-Selinger, C. Hopf, C. Sun, and W. Jacob, J. Nucl. Mater. **363–365**, 174 (2007).
[30]Y. A. Mankelevich, M. A. Olevanov, and T. V. Rakhimova, Plasma Sources Sci. Technol. **17**, 015013 (2008).
[31]I. Géraud-Grenier, V. Massereau-Guilbaud, and A. Plain, Eur. Phys. J. Appl. Phys. **8**, 53 (1999).
[32]H. Kersten, H. Deutsch, and G. M. W. Kroesen, Int. J. Mass Spectrom. **233**, 51 (2004).
[33]M. Mikikian, M. Cavarroc, L. Couëdel, Y. Tessier, and L. Boufendi, Pure Appl. Chem. **82**, 1273 (2010).
[34]S. K. Zhdanov, M. Schwabe, R. Heidemann, R. Sütterlin, H. M. Thomas, M. Rubin-Zuzic, H. Rothermel, T. Hagl, A. V. Ivlev, G. E. Morfill, V. I. Molotkov, A. M. Lipaev, O. F. Petrov, V. E. Fortov, and T. Reiter, New J. Phys. **12**, 043006 (2010).
[35]C. Arnas, A. Michau, G. Lombardi, L. Couëdel, and K. Kumar K, Phys. Plasmas **20**, 013705 (2013).
[36]V. Bouchat, O. Feron, B. Gallez, B. Masereel, C. Michiels, T. V. Borght, and S. Lucas, Surf. Coat. Technol. **205**, S577 (2011).
[37]M. Schulze, D. O'Connell, T. Gans, P. Awakowicz, and A. v. Keudell, Plasma Sources Sci. Technol. **16**, 774 (2007).
[38]S. A. Khrapak, A. V. Ivlev, G. E. Morfill, and H. M. Thomas, Phys. Rev. E **66**, 046414 (2002).
[39]D. Samsonov and J. Goree, IEEE Trans. Plasma Sci. **27**, 76 (1999).
[40]K. Avinash, A. Bhattacharjee, and S. Hu, Phys. Rev. Lett. **90**, 075001 (2003).
[41]Z. Hu, Y. Chen, X. Zheng, F. Huang, G.-f. Shi, and M. Y. Yu, Phys. Plasmas **16**, 063707 (2009).
[42]W. J. Goedheer and V. Land, Plasma Phys. Controlled Fusion **50**, 124022 (2008).
[43]W. J. Goedheer, V. Land, and J. Venema, Contrib. Plasma Phys. **49**, 199 (2009).
[44]E. G. Wang, Z. G. Guo, J. Ma, M. M. Zhou, Y. K. Pu, S. Liu, G. Y. Zhang, and D. Y. Zhong, Carbon **41**, 1827 (2003).
[45]K. Tachibana, T. Mukai, A. Yuuki, Y. Matsui, and H. Harima, Jpn. J. Appl. Phys. **29**, 2156 (1990).
[46]J. Perrin, C. Bohm, R. Etemadi, and A. Lloret, Plasma Sources Sci. Technol. **3**, 252 (1994).
[47]V. Land and W. J. Goedheer, New J. Phys. **9**, 246 (2007).
[48]C. Hollenstein, Plasma Phys. Controlled Fusion **42**, R93 (2000).